

EFFECT OF TAILCONE SHAPE ON HOT STREAK PHENOMENA AND INFRARED SIGNATURE OF SERPENTINE NOZZLE WITH AFT DECK

Jiazheng Fan, Qingzhen Yang, Xubo Du, Haoqi Yang, Yubo He, Yongqiang Shi

School of Power and Energy, Northwestern Polytechnical University, Xi'an 710072, China

Abstract

To reduce the infrared signature behind and below the aircraft, serpentine nozzles with aft deck are widely used in modern military aircraft. At the inlet of the nozzle, the core flow passing through the tailcone will generate the central vortex. The secondary flow caused by the central vortex will affect the temperature distribution of the flowfield within the serpentine nozzle, resulting in the hot streak on the nozzle wall, which has an adverse impact on the thermal protection of the nozzle. Therefore, this paper aims to numerically investigate the effect of tailcone shape on the hot streak phenomena and the infrared signature of the serpentine nozzle with aft deck. In this paper, serpentine nozzles with aft deck are designed based on curvature control regulation, and four tailcones with different shapes are designed by power curves. Computational Fluid Dynamics (CFD) simulations are conducted to obtain the temperature distribution of the nozzle, and Reverse Monte Carlo Method (RMCM) is applied to study the infrared signature of the nozzle in the $3\mu\text{m}$ - $5\mu\text{m}$ band. The results show that, for the cases without engine swirl, the hot streak area on the nozzle wall and the infrared radiation intensity of the nozzle rise with the increase of the tailcone surface curvature, in which the infrared signature level at the positive azimuth angle in the vertical plane is greater than that at the negative azimuth angle; For the cases with engine swirl, the change of tailcone curvature has little effect on the hot streak, but the serpentine nozzle with large curvature tailcone has lower infrared radiation intensity. The research results can provide guidance for the thermal management and stealth design of the serpentine nozzle.

Keywords: serpentine nozzle, aft deck, infrared signature, hot streak, tailcone

1. Introduction

With the rapid development of infrared detection technology, the threat of infrared detection systems and infrared-guided missiles to aircraft is becoming more and more serious, and the exhaust system is the primary infrared radiation source of aircraft [1-4]. In the past, many scholars have studied the infrared suppression methods of the exhaust system. The serpentine nozzle has turned out to be an effective way because of its special advantages in suppressing the infrared signature. Crowe et al. [5] studied the effects of the serpentine nozzle geometry and engine swirl on nozzle temperature distribution. The results showed that the tailcone vortex and the curved shape of the serpentine nozzle led to the formation of the hot streak, and the engine swirl affected the distribution of hot streak. Subsequently, Crowe et al. [6] established a set of hot streak characterization parameters to quantify the hot streak of the nozzle. The results showed that compared with the geometry of the serpentine nozzle, the engine swirl had a more significant effect on the outlet temperature distribution. The smaller the white number was, the more obvious the hot streak phenomenon of the serpentine nozzle was. Cheng et al. [7] investigated the effect of engine swirl on the infrared characteristics of the serpentine nozzle. The results showed that the location and intensity of the hot streak varied with increasing swirl angle, which induced changes in the self-radiance from the nozzle wall; The engine swirl could effectively suppress the infrared characteristics of the serpentine nozzle. Compared with the case without vortex, the total IRSL (infrared signature level) on the vertical plane was reduced by 13.9% when the swirl angle was 10° . Gao et al. [8] analyzed the influence of the outlet shape on the exhaust system's infrared radiation (IR) characteristics. The results showed that the double S-shaped

nozzle could reduce the infrared signal of the target effectively. The models with trapezoid outlet shapes had significantly lower IR intensity than the double S-shaped nozzles with other outlet shapes and could reduce the peak of IR intensity by at least 70% compared with the axis-symmetric nozzle. Gao et al. [9] used the improved reverse Monte Carlo method to analyze the infrared characteristics of flying wing UAVs (unmanned aerial vehicles) with different exhaust systems in 3~5 μm and 8~14 μm bands. The results showed that compared with the UAV with a single serpentine exhaust system, the UAV with a double serpentine exhaust system had a lower infrared radiation intensity. Cheng et al. [10,11] analyzed the influence of the shield ratio on the IR signature of a serpentine nozzle. Results showed that the shield ratio had a significant influence on the infrared signature of the serpentine nozzle, the visible area ratio was suggested to be under 0.041.

On some military aircraft, an area of the fuselage called the aft deck is placed downstream of the exhaust exit to provide further line-of-sight denial and thermal management. Rajkumar et al. [12] conducted an experimental study on the flow characterization for a shallow single serpentine nozzle with aft deck. The results showed that the presence of the aft deck prevented the formation of barrel shocks, which was conducive to reducing the infrared signature of the serpentine nozzle. Mohamed Abdelmotalib et al. [13] studied the effects of the shape and length of the annular mixer on the temperature distribution of the two-dimensional nozzle with aft deck. The results demonstrated that the reduction in mixer length could decrease the temperature inside and outside the nozzle, which could reduce infrared radiation; A mixer with a smaller diameter and shorter length with a cylindrical shape could provide better performance for a nozzle.

Above results have shown that the tailcone vortex and the curved shape of the serpentine nozzle led to the hot streak phenomenon. Previous studies on serpentine nozzle mainly focused on the effects of geometry and inlet swirl on its temperature distribution and infrared signature, while the effects of tailcone shape on the temperature distribution and infrared signature of the serpentine nozzle have not been reported in the public literature. And few studies pay attention to the influence of the existence of the aft deck on the infrared signature of the serpentine nozzle. Therefore, the main purpose of this paper is to study the influence of the tailcone shape on the hot streak phenomenon and the infrared signature of the serpentine nozzle with aft deck. The research results can provide further guidance for the thermal management and stealth design of the serpentine exhaust system.

2. Geometry of exhaust system

Figure 1 shows the geometry of the serpentine exhaust system with aft deck studied in this paper, which consists of an entrance section, a convergent section, a divergent section and an aft deck. The entrance section contains a core inlet, a bypass inlet, a tailcone and an annular mixer.

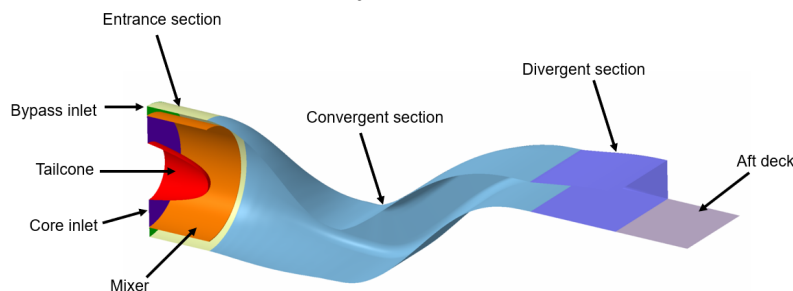


Figure 1 – Geometry of the serpentine exhaust system with aft deck.

The C++ program based on curvature control is developed to generate the profile of the convergent section of the serpentine nozzle. The program can realize a good transition of the nozzle from circular inlet to rectangular outlet, and control the shape of the middle section at the junction of the first and second bends of the double serpentine nozzle. The change law of nozzle centerline and area is based on the Lee curve[14]. The centerline and area change law of the first S-bend of the double serpentine nozzle studied in this paper is shown in equations 1 and 2, the center line and area change law of the second S-bend is shown in equations 3 and 4, where y and A represent the center offset

and area of the cross-section at position x . Δy is the center offset of nozzle inlet and outlet; L is the total length of the convergent section of the serpentine nozzle; A_{in} and A_{out} are the inlet and outlet area of the convergent section of the nozzle. The expansion section of the serpentine nozzle is designed by the method of characteristic[15]. The sidewall and lower wall of the expansion section are straight sections. The aft deck is a straight section, which is connected with the lower wall of the expansion section.

$$y = \Delta y \left(-2 \left(\frac{x}{L} \right)^3 + 3 \left(\frac{x}{L} \right)^2 \right) \tag{1}$$

$$\frac{A}{A_{in}} = \left(\frac{A_{out}}{A_{in}} - 1 \right) \left[-2 \left(\frac{x}{L} \right)^3 + 3 \left(\frac{x}{L} \right)^2 \right] + 1 \tag{2}$$

$$y = \Delta y \left(3 \left(\frac{x}{L} \right)^4 - 8 \left(\frac{x}{L} \right)^3 + 6 \left(\frac{x}{L} \right)^2 \right) \tag{3}$$

$$\frac{A}{A_{in}} = \left(\frac{A_{out}}{A_{in}} - 1 \right) \left[3 \left(\frac{x}{L} \right)^4 - 8 \left(\frac{x}{L} \right)^3 + 6 \left(\frac{x}{L} \right)^2 \right] + 1 \tag{4}$$

The serpentine nozzle is designed to completely shield the high-temperature core flow and the tailcone, which indicates that the annular mixer and the high-temperature parts inside the annular mixer are invisible from all directions at the rear of the serpentine nozzle. The geometry parameters of the serpentine nozzle with aft deck studied in this paper are shown in Figure 2, and the dimensionless values of these parameters are shown in Table1.

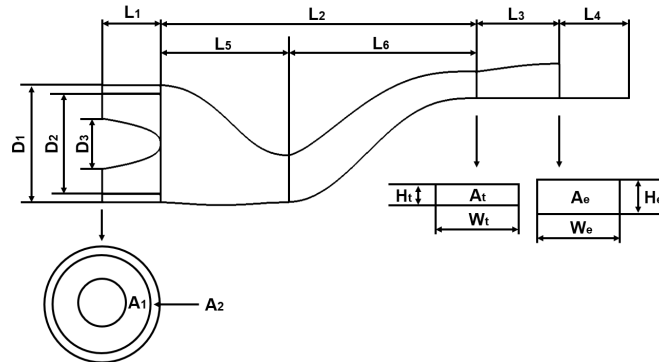


Figure 2 – Geometry parameters of the serpentine nozzle with aft deck.

Table 1. Dimensionless values of geometry parameters.

Dimensionless parameters	Value
L_1/D_1	0.5
L_2/D_1	2.7
L_3/D_1	0.71
L_4/H_e	2
L_5/D_1	1.08
L_6/D_1	1.62
D_2/D_1	0.848
D_3/D_1	0.432
W_t/H_t	6
W_e/H_e	4.65
W_t/W_e	1
$A_t/(A_1+A_2)$	0.74
$A_e/(A_1+A_2)$	0.956

The shape of the engine tailcone studied in this paper is constructed by the power function curve. Its expression is defined as follows:

$$y=L_c(2x/D_3)^n \quad (5)$$

where L_c is the axial length of tailcone, in this paper, $L_c = L_1$ and n is the power of the power curve. Four tailcone shapes with n of 2, 3, 4 and 5 are studied, and their profiles are shown in Figure 3.

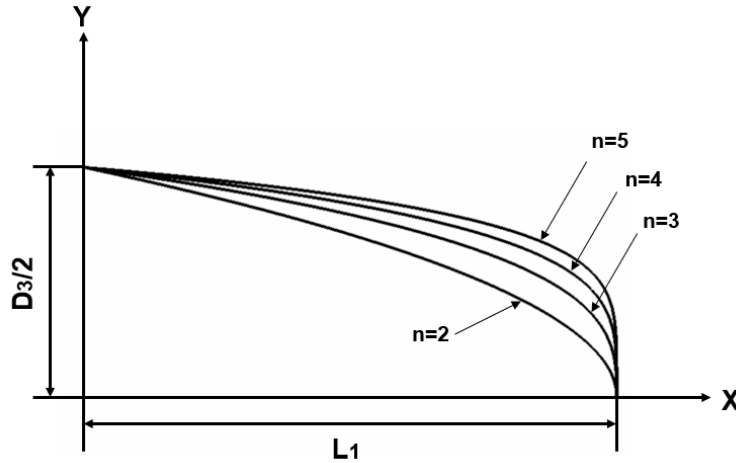


Figure 3 – Geometry of tailcone.

3. Numerical simulation method

3.1 The computational fluid dynamics numerical method

In this paper, the computational grids are structured grids created by using ICEM, and the grids near the nozzle wall are properly densified to make $y^+ < 2$. The size of the computational domain is $30D_1 \times 10D_1 \times 10D_1$, as shown in Figure 4. Three sets of grids containing 3.5 million, 7 million and 10.5 million elements are selected to verify grid independence, which refers to coarse grids, medium grids and fine grids, respectively. The comparison of the dimensionless static pressure distribution of the upper and lower walls of the nozzle symmetry plane is given in Figure 5, where P_b is the ambient pressure. It can be seen that the static pressure distribution of the upper and lower walls of the serpentine nozzle with 7 million and 10.5 million elements is almost the same. Therefore, the grid with 7 million elements is used for flow features analysis of the serpentine nozzle studied in this paper.

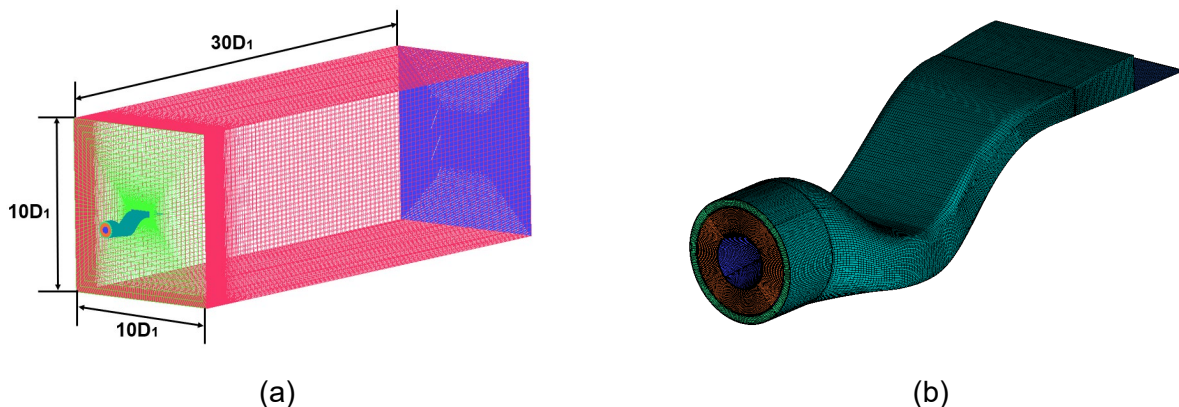


Figure 4 – The grids of computational domain and nozzle: (a) computational domain, (b) grids of the serpentine nozzle.

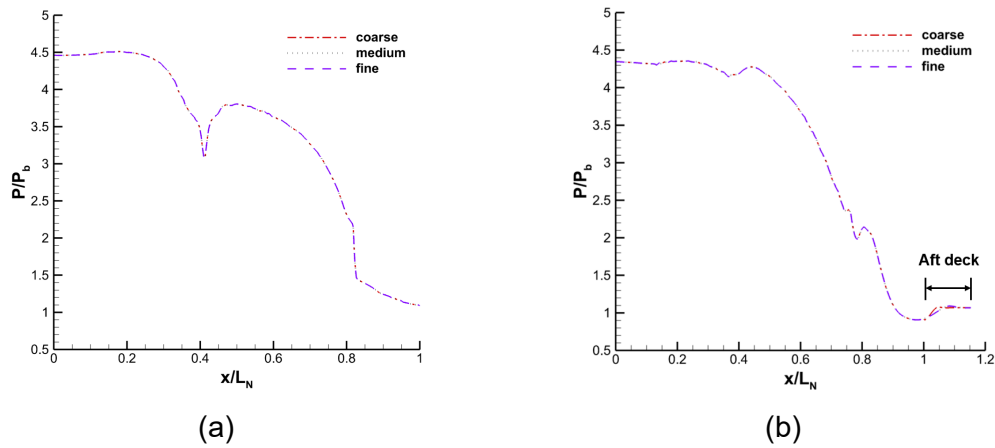


Figure 5 – The dimensionless static pressure of serpentine nozzle for different grid sizes: (a) dimensionless static pressure distribution of the upper wall, (b) dimensionless static pressure distribution of the lower wall.

The flowfield of the serpentine exhaust system model with aft deck was simulated by using ANSYS FLUENT, the equations solved were the fully 3D, compressible, steady, Reynolds-averaged Navier–Stokes equations. The participation of CO_2 , CO , H_2O , O_2 and N_2 were taken into account. The shear stress transport $k-\omega$ model considering compressible effect was adopted as the turbulence model, which was verified in sun’s research[16]. In terms of boundary conditions, the bypass inlet was set as the pressure inlet, with a total pressure of 213737.5 Pa and a total temperature of 401.04 K. The molar fractions of O_2 and N_2 at the bypass inlet were set to be 23.3% and 76.7%, respectively. The core inlet was set as the pressure inlet, with a total pressure of 213737.5 Pa and a total temperature of 977.59 K. The molar fractions of CO_2 , CO and H_2O at the core inlet were set to be 7.18%, 0.01% and 2.94%, respectively. The far-field boundary condition used the pressure far-field, with a pressure of 46563 Pa and a temperature of 249 K. The walls were all set as no-slip walls.

3.2 The infrared signature numerical method

In this paper, the infrared signature calculation program developed based on the reverse Monte Carlo method was used to calculate the infrared radiation intensity and spatial distribution of the serpentine nozzle model. This program is developed based on the C++ platform, and can separate solid and gas radiation from total infrared radiation, which is helpful in exploring the infrared radiation mechanism of the serpentine nozzle with aft deck studied in this paper. A schematic of the RMCM is shown in Figure 6. Its basic principle is to randomly emit characteristic rays from the detector to the target, track the rays in reverse, and judge whether they are absorbed in the transmission process until they are absorbed or escape from the transparent boundary. Then, taking the escape point and absorption point as the starting point, the infrared radiation transmission is inversely calculated along the characteristic line. Finally, the infrared signature received by the target in the detector is obtained.

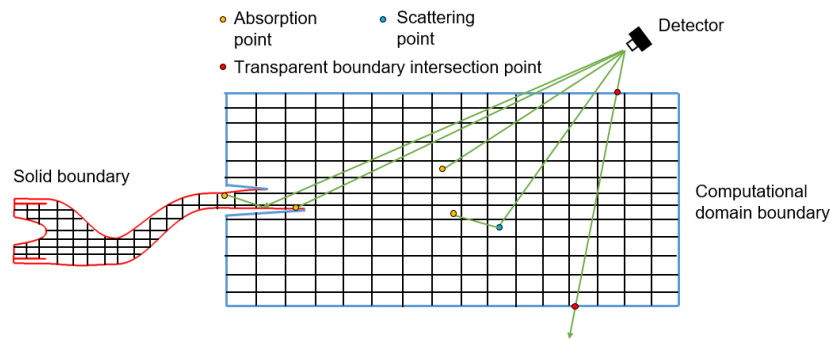


Figure 6 – Ray tracing principle of RMCM.

The infrared signature of the serpentine nozzle with aft deck was calculated in the 3~5 μm band. The emissivity of the solid wall was set as 0.85. Thirty-seven detection points were placed in the horizontal and vertical detection planes, respectively, and the azimuth on the two planes ranged from -90° to 90°, as shown in Figure 7. The wall temperature distribution of the nozzle, temperature and pressure of gas and infrared active gas component concentration distribution required for infrared radiation calculation can be obtained from CFD simulation.

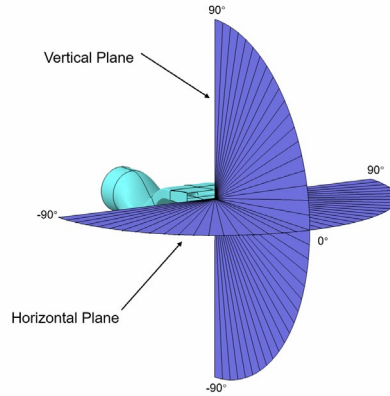


Figure 7 – Detection angle distribution of infrared detector.

A disk was selected to verify the reliability of the infrared signature calculation program. The disk used for verification had a radius of 1m, an emissivity of 1.0 and a surface temperature of 400K. The comparison between the numerical results and the theoretical results for the 3~5 μm band is shown in Figure 8. The comparison of the spatial distribution of the infrared radiation intensity of the disk obtained by numerical calculation and theoretical calculation shows that the infrared radiation intensity calculation program used in this paper is reliable.

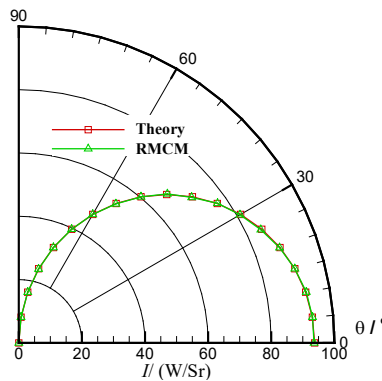


Figure 8 – Comparison of RMCN results with theoretical values of integral infrared radiation intensity in a circular plane.

4. Results

The engine swirl angle is defined as the angle between the tangential flow component of the turbine exit velocity vector and the axial vector, which is a flow condition deemed necessary to simulating a realistic turbofan engine flowfield. In this paper, the engine swirl angle is taken as 10°, and the engine swirl is introduced through the pressure inlet boundary condition of the core section. The effects of four different tailcone shapes on the temperature distribution of serpentine nozzle with aft deck are studied in this paper, and the infrared signature of nozzles with different tailcone shapes are compared.

4.1 Cases without engine swirl

Figure 9 shows the wall temperature distribution of serpentine nozzles with four different tailcone

shapes without engine swirl. For these four cases, the hot streak phenomenon appears on the upper and lower wall surfaces of the nozzle, and the temperature and area of the hot streak along the flow direction of the gas increase. In addition, the temperature near the centerline of the upper wall of the nozzle is significantly lower than that on both sides of the centerline, while the hot streak on the lower wall and the aft deck of the nozzle appears near the centerline of the lower wall and the aft deck. With the increase of the tailcone surface curvature, the temperature and area of the hot streak on the upper wall of the nozzle increase, and the temperature and area of the hot streak on the lower wall and the aft deck of the nozzle first increase and then decrease. For the case of $n=4$, the hot streak temperature reaches the peak value, as shown in Table 2. Figure 10 shows the gas temperature distribution at different cross-sections in the serpentine nozzle. It can be seen that with the increase of the tailcone surface curvature, the high-temperature core flow gradually breaks through the package of the bypass flow and impinges on the nozzle wall. This phenomenon is most apparent when $n=4$.

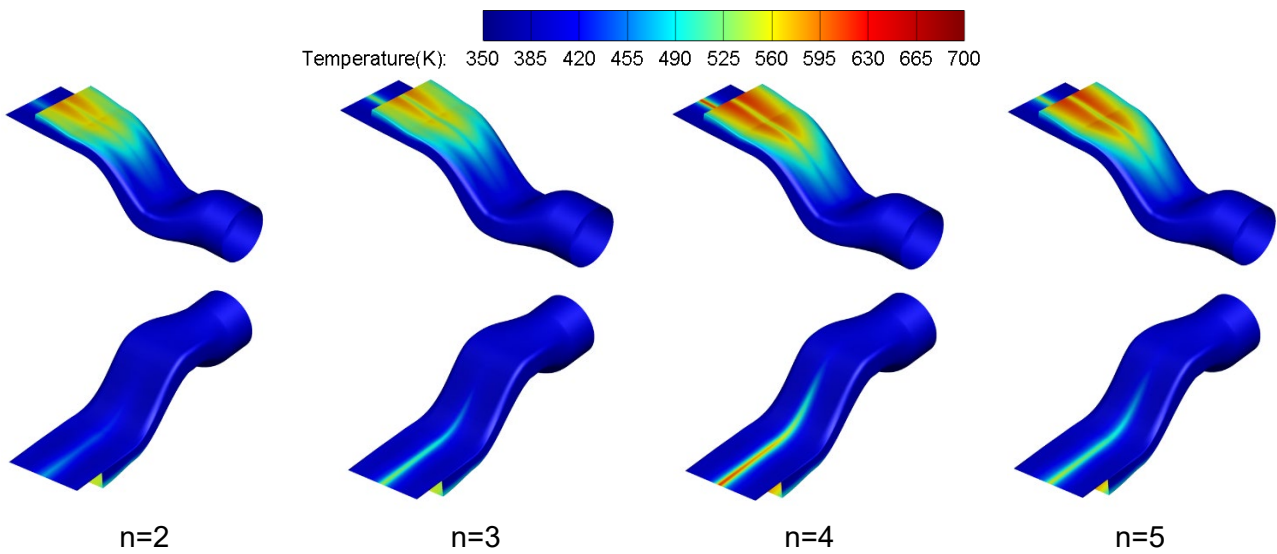


Figure 9 – Wall temperature distribution of serpentine nozzle with different tailcone shape without engine swirl.

Table 2. Maximum temperature of nozzle wall (without engine swirl).

Cases	n=2	n=3	n=4	n=5
Maximum temperature of upper wall (K)	589	591	615	614
Maximum temperature of lower wall and aft deck (K)	468	542	612	553

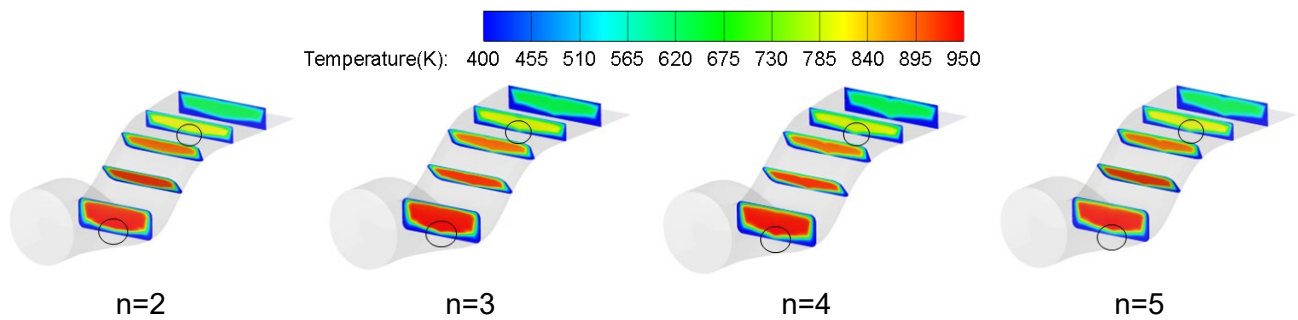


Figure 10 – Temperature distribution at different cross-sections in the serpentine nozzle.

In order to explore the reasons for the above differences in the gas temperature distribution within the nozzle, 3D streamlines near the tailcone are given. As shown in Figure 11, the streamlines are colored with the vorticity component in Z direction (perpendicular to the cross-section of the nozzle

outlet). It can be seen that with the increase of the surface curvature of the tailcone, the flow separation behind the tailcone becomes more and more serious, and a pair of counter-rotating vortices appear behind the tailcone, which is called tailcone vortex. The intensity of the tailcone vortex increases with the rise of the tailcone surface curvature and reaches the maximum when $n=4$. The increase of tailcone vortex strength further enhances the mixing of the core flow and the bypass flow, and the core flow is dragged gradually toward the lower wall of the nozzle until it breaks through the package of the bypass flow and impinges on the nozzle wall, resulting in the difference in the temperature and area of the hot streak on the nozzle wall as shown in Figure 9.

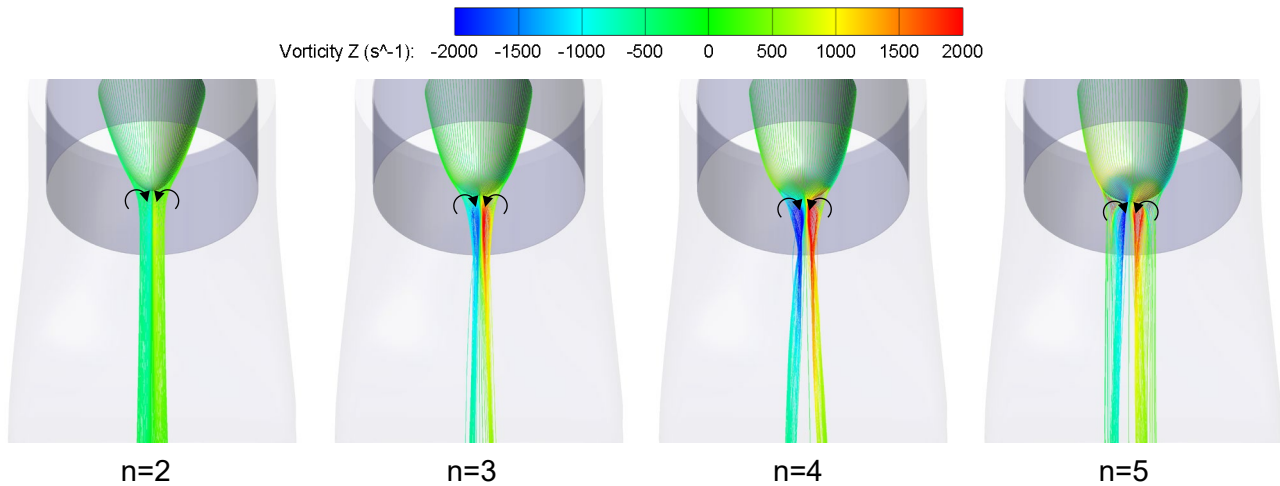


Figure 11 – 3D streamlines near the tailcone (without engine swirl).

The difference in temperature and area of the hot streak will also lead to the difference in the infrared signature of the nozzle. Figure 12 shows the dimensionless integral infrared radiation intensity in the horizontal and vertical detection planes of four different tailcone shapes of the serpentine nozzle with aft deck when engine swirl does not exist. Where I_{\max} represents the maximum integral infrared radiation intensity of all cases studied in this paper, "Total" represents the total integral infrared radiation intensity, "Solid" represents the solid integral infrared radiation intensity, "Gas" represents the gas integral infrared radiation intensity. As shown in Figure 12 (a), in the horizontal detection plane, the cases with different tailcone shapes show significant differences. The angular mean value of the total integral infrared radiation intensity of the case $n=4$ increases by 10.78% compared with the case $n=2$. This difference in the total integral infrared radiation intensity is mainly caused by the solid integral infrared radiation intensity. The angular mean value of the solid integral infrared radiation intensity in the case $n=4$ increases by 32.37% compared with the case $n=2$. Therefore, the increase in hot streak temperature and area caused by the increase in tailcone vortex intensity can significantly affect the infrared radiation characteristics in the horizontal detection plane of the serpentine nozzle.

As shown in Figure 12 (b), in the vertical detection plane, the total integral infrared radiation intensity of all four cases shows an asymmetric distribution. The infrared radiation intensity at the negative detection angle is significantly lower than that at the positive detection angle. The reason for this phenomenon is the shielding effect of the aft deck on the high-temperature wall and plume of the serpentine nozzle. Due to the existence of the aft deck, the solid integral infrared radiation intensity within the detection angle range of -20° to -90° is minimal. The solid integral infrared radiation intensity at the positive detection angle is relatively large due to the hot streak on the aft deck and is obviously affected by the tailcone shape. The mean value of the solid integral infrared radiation intensity in the vertical detection plane of the case $n=4$ is increased by 63.84% compared with the case $n=2$, and the total integral infrared radiation intensity is increased by 7.37%. In addition, there is a peak area of solid integral infrared radiation intensity within the range of 0° to -20° of the vertical detection plane. This is because the high-temperature hot streak on the upper wall of the nozzle can

be directly observed within this detection angle range. With the further reduction of the detection angle, the aft deck gradually blocks the high-temperature area, resulting in the rapid decline of solid integral infrared radiation intensity.

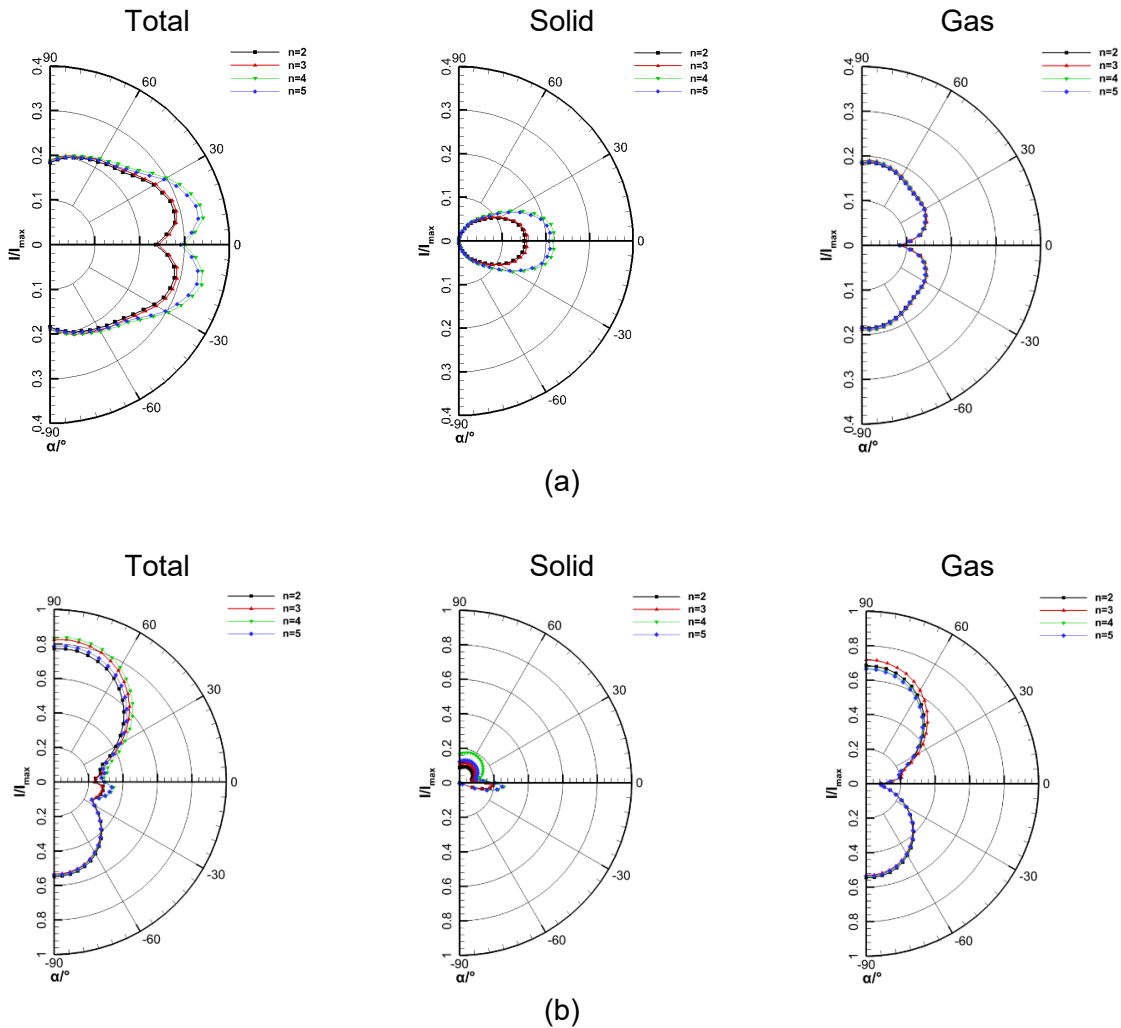


Figure 12 – Dimensionless integral infrared radiation intensity polar curves of four different tailcone shapes of serpentine nozzle with aft deck when engine swirl does not exist: (a)horizontal plane, (b)vertical plane.

4.2 Cases with engine swirl

Figure 13 shows the wall temperature distribution of serpentine nozzles with four different tailcone shapes with engine swirl. For these four cases, the hot streak appears on the left side of the upper wall of the nozzle (looking along the flow direction), and the temperature and area of the hot streak are larger than those without engine swirl. In addition, the temperature and area of the wall hot streak increase along the flow direction, and the hot streak also appears on the left wall of the nozzle expansion section. The hot streak on the lower wall and the aft deck of the nozzle appears on the right side of the lower wall and the aft deck, and its area is more extensive than that in the no-swirl cases. Figure 14 shows the temperature distribution at different cross-sections in the serpentine nozzle with engine swirl. It can be seen that the asymmetric distribution of the hot streak on the nozzle wall is closely related to the direction of the engine swirl. Due to the existence of the clockwise engine swirl (looking along the flow direction), the high-temperature core flow is dragged to the upper left and lower right, impacting the left side of the upper wall and the right side of the lower wall of the nozzle respectively, thus forming the hot streak distribution shown in Figure 13.

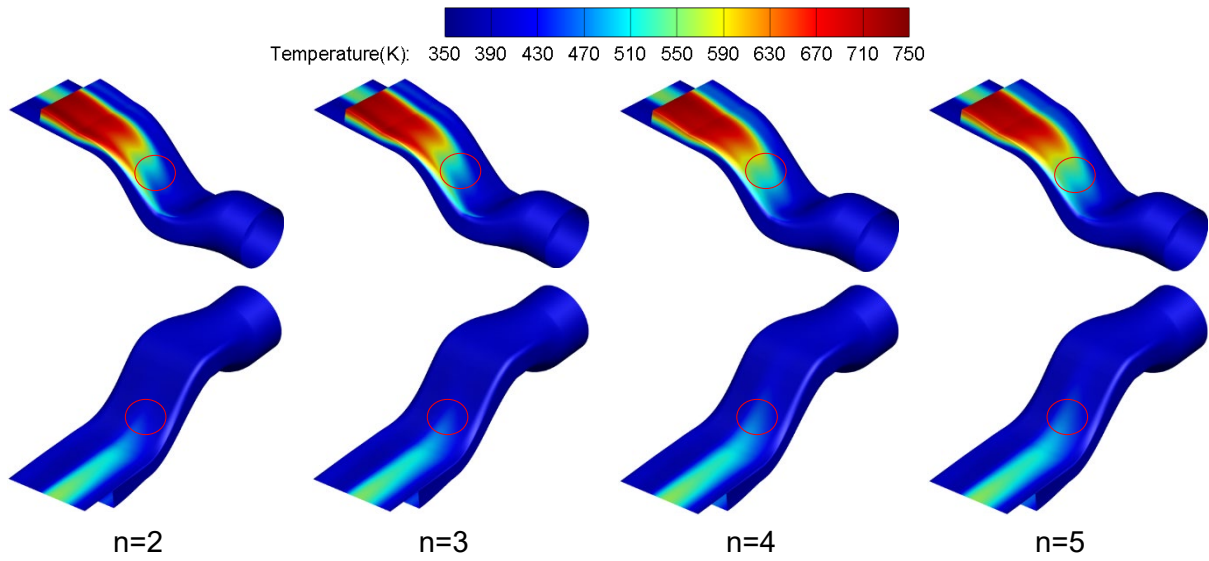


Figure 13 – Wall temperature distribution of serpentine nozzle with different tailcone shapes with engine swirl.

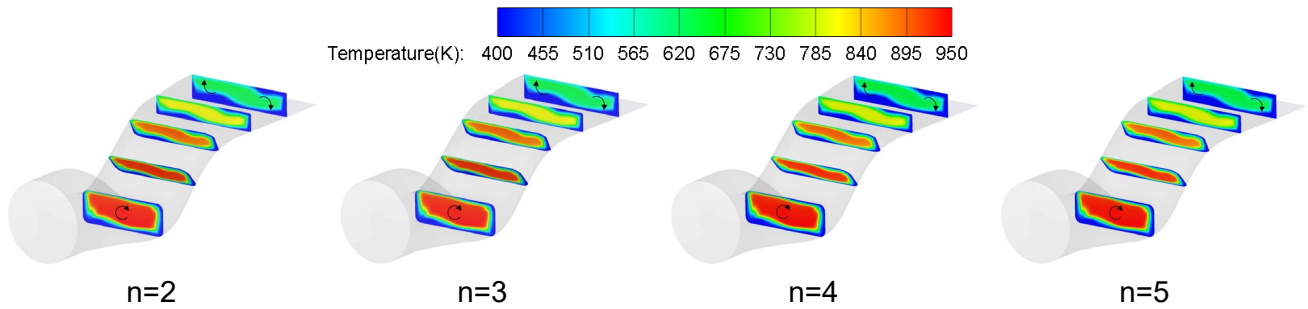


Figure 14 – Temperature distribution at different cross-sections in the serpentine nozzle.

When the engine swirl exists, the change of tailcone curvature has little effect on the hot streak temperature on the upper and lower walls of the nozzle and the aft deck. As shown in Table 3, the peak temperature difference of the nozzle wall in different cases is very slight. However, with the increase of the tailcone curvature, the area of the sub-high-temperature region on the upper and lower walls increases slightly. This is because when the engine swirl exists, the strength of the tailcone vortex increase with the increase of the tailcone surface curvature, as shown in Figure 15, which will intensify the mixing of core flow and bypass flow, increasing the area of the sub-high-temperature region.

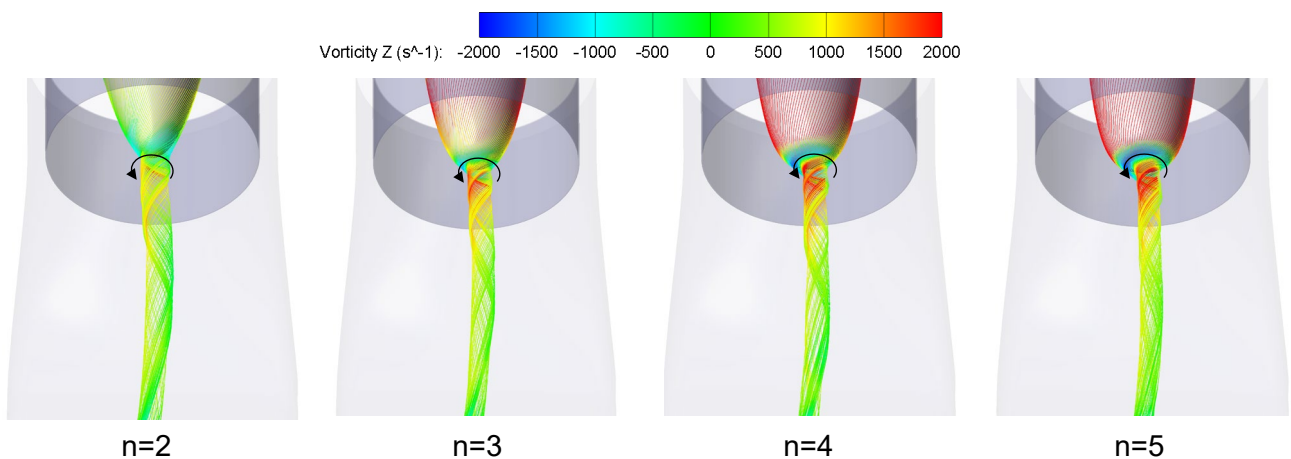


Figure 15 – 3D streamlines near the tailcone (with engine swirl).

Table 3. Maximum temperature of nozzle wall (with engine swirl).

	n2	n3	n4	n5
Maximum temperature of upper wall (K)	738	733	726	723
Maximum temperature of lower wall and aft deck (K)	561	557	562	562

Figure 16 shows the dimensionless integral infrared radiation intensity in the horizontal and vertical detection planes of four different tailcone shapes of the serpentine nozzle with aft deck when engine swirl exists. As shown in Figure 16 (a), the total integral infrared radiation intensity in the horizontal detection plane of all four cases shows an asymmetric distribution, and the integral radiation intensity at the negative azimuth is significantly higher than that at the positive potential angle. By observing the solid integral radiation intensity curves, it can be seen that this is mainly caused by the asymmetry of the hot streak on the nozzle wall when the engine swirl exists. The high-temperature hot streak on the sidewall of the nozzle can be observed from the negative azimuth, which leads to the increase of the solid infrared radiation intensity at the negative azimuth, and then leads to the increase of the total infrared radiation intensity at the negative azimuth. As shown in Figure 16 (b), in the vertical detection plane, the integral infrared radiation intensity of all four cases shows an asymmetric distribution similar to that of cases without swirl, which is mainly caused by the shielding effect of the aft deck.

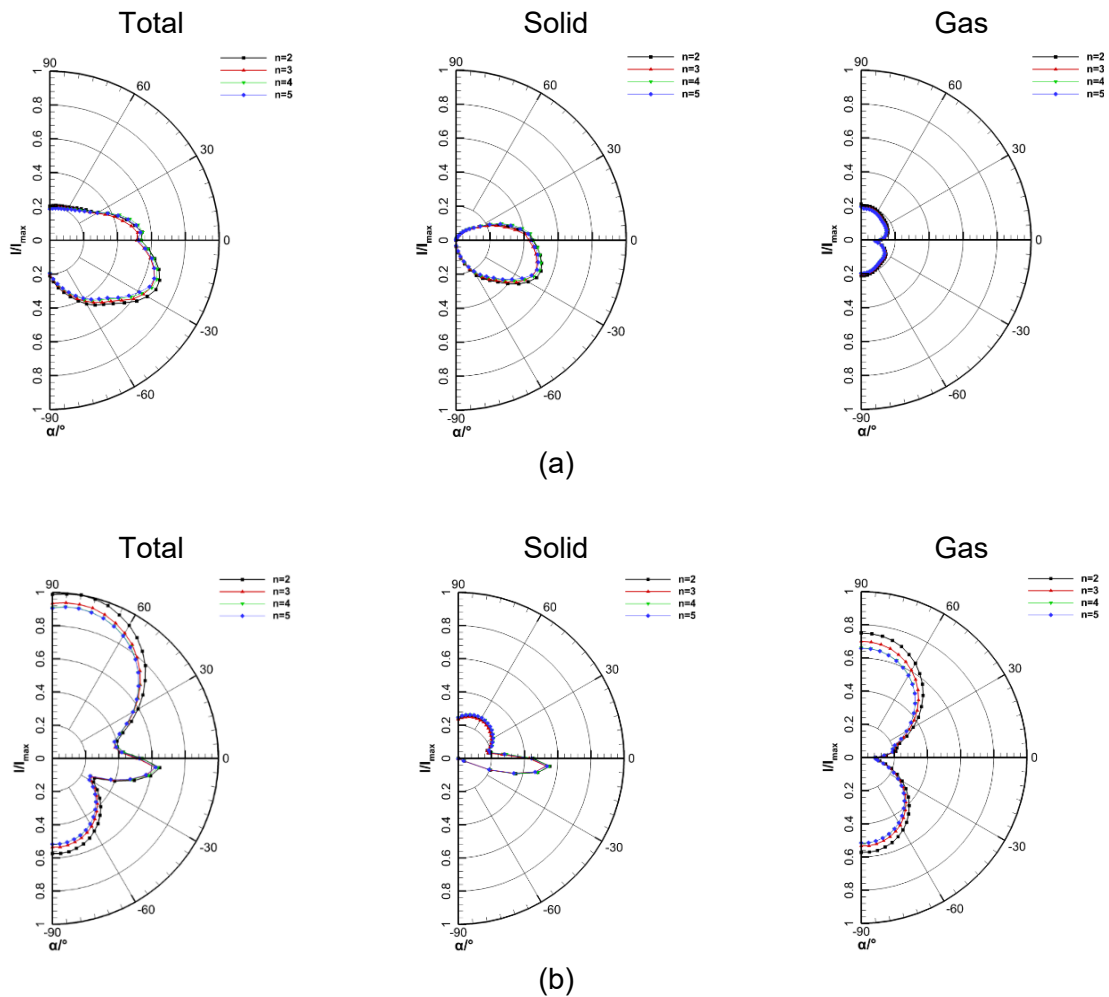


Figure 16 – Dimensionless integral infrared radiation intensity polar curves of four different tailcone shapes of serpentine nozzles with aft deck when engine swirl exists: (a)horizontal plane, (b)vertical plane.

In addition, by comparing the gas infrared radiation intensity with different tailcone shapes in the two detection planes, it can be found that the gas integral radiation intensity increases with the decrease of the tailcone surface curvature. Among them, compared with the case $n=5$, the gas integral infrared radiation intensity of the case $n=2$ increases by 7.21% in the horizontal detection plane, 12.76% in the vertical detection plane, and the total integral infrared radiation intensity increases by 5.7% and 8.31% respectively. The gas isosurface of 620K shown in Figure 17 explains the causes of the above phenomena. With the increase of the tailcone curvature, the mixing of core flow and bypass flow becomes stronger, resulting in the reduction of the size of the high-temperature core plume, thus reducing the gas infrared radiation intensity and finally reducing the total infrared radiation intensity.

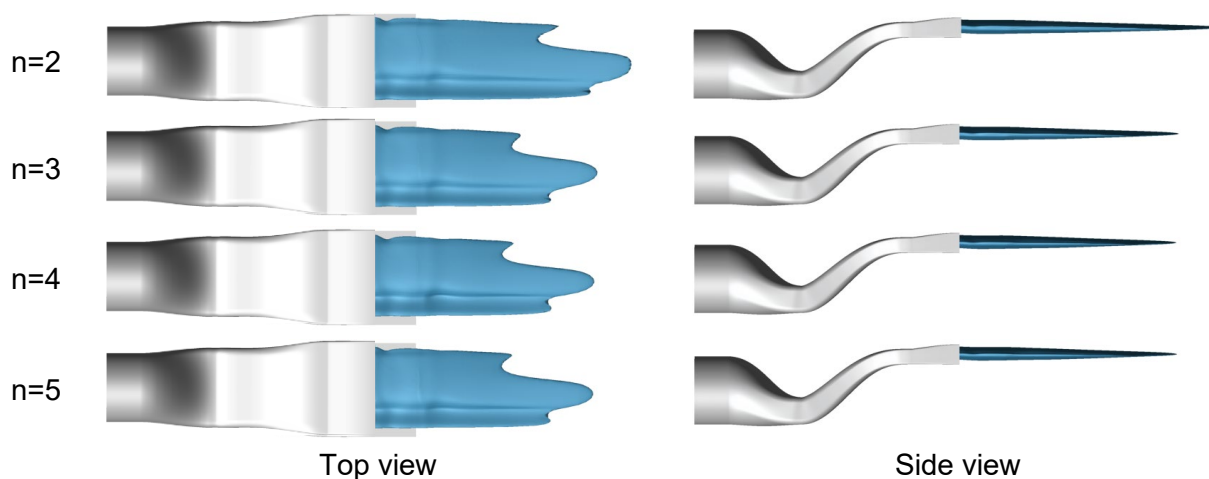


Figure 17 – Gas isosurface of 620K (with engine swirl).

5. Conclusions

In this paper, the hot streak phenomenon of the serpentine nozzle with aft deck with different tailcone shapes was numerically simulated, and the influence of tailcone shapes on the infrared signature of the nozzle in $3\sim 5\mu\text{m}$ band was compared. The main conclusions are as follows:

For the cases without engine swirl, with the increase of the tailcone surface curvature, the strength of the tailcone vortex also increases, and the high-temperature core flow gradually breaks through the package of the bypass flow and impinges on the nozzle wall, increasing the temperature and area of the hot streak on the nozzle wall. The increase in nozzle wall temperature leads to the increase in the solid infrared radiation intensity of the nozzle, which leads to the increase in total infrared radiation signature. Compared with the case $n=2$, the solid integral infrared radiation intensity of the case $n=4$ in the horizontal detection plane increases by 32.37%, and the total integral infrared radiation intensity increases by 10.78%; In the vertical detection plane, the solid integral infrared radiation intensity increases by 63.84%, and the total integral infrared radiation intensity increases by 7.37%.

For the cases with engine swirl, the temperature and area of the hot streak on the serpentine nozzle wall are insensitive to the change of the tailcone surface curvature. However, with the increase in the tailcone surface curvature, the mixing of core flow and bypass flow becomes stronger, which leads to the reduction of the size of the high-temperature core plume. Thus, the total infrared radiation intensity of the nozzle is reduced. Compared with the case $n=5$, the gas integral infrared radiation intensity of the case $n=2$ in the horizontal detection plane increases by 7.21%, the total integral infrared radiation intensity increases by 5.7%, the gas integral infrared radiation intensity in the vertical detection plane increases by 12.76%, and the total integral infrared radiation intensity increases by 8.31%.

6. Contact Author Email Address

mailto: jzfan@mail.nwpu.edu.cn

7. Copyright Statement

The authors confirm that they, and/or their company or organization, hold copyright on all of the original material included in this paper. The authors also confirm that they have obtained permission, from the copyright holder of any third-party material included in this paper, to publish it as part of their paper. The authors confirm that they give permission, or have obtained permission from the copyright holder of this paper, for the publication and distribution of this paper as part of the ICAS proceedings or as individual off-prints from the proceedings.

Acknowledgements

The authors would like to express their gratitude for the financial support of the Natural Science Basic Research Program of Shaanxi (Program No.2022JQ-052).

References

- [1] Mahulikar S P, Sonawane H R, Rao G A. Infrared signature studies of aerospace vehicles. *Progress in aerospace sciences*, Vol. 43, pp 218-245, 2007.
- [2] Rao G A, Mahulikar S P. Integrated review of stealth technology and its role in airpower. *The aeronautical journal*, Vol. 106, No.2751, pp 629-642, 2002.
- [3] Johansson M, Dalenbring M. Calculation of IR signatures from airborne vehicles. *Modeling and Simulation for Military Applications*, Vol. 106, No.6228, pp 369-380, 2006.
- [4] Johansson M. Propulsion Integration in an UAV. *24th AIAA Applied Aerodynamics Conference*, San Francisco, California Vol. 6228, pp 369-380, 2006.
- [5] D. S. and C. L. Effect of Geometry on Exit Temperature from Serpentine Exhaust Nozzles. *53rd AIAA Aerospace Sciences Meeting*, Kissimmee, Florida, AIAA-2015-1670,2015.
- [6] D. S. Crowe and C. L. Martin. Hot Streak Characterization of High-Performance Double-Serpentine Exhaust Nozzles at Design Conditions. *Journal of Propulsion and Power*, Vol. 35, No. 3, pp 501-511, 2019.
- [7] W. Cheng, Z. Wang, L. Zhou, J. Shi, and X. Sun. Infrared signature of serpentine nozzle with engine swirl. *Aerospace Science and Technology*, Vol. 86, pp 794-804, 2019.
- [8] Gao Xiang, Yang Qingzhen, Shi Yongqiang, Wang Yun, Yang Huicheng. Numerical simulation of radiation intensity of double S-shaped exhaust system with different outlet shapes. *Infrared and Laser Engineering*, Vol. 44, No. 6, pp 1726-1732, 2015.
- [9] Gao X, Yang Q, Yang H, et al. An Improved Reverse Monte Carlo Method for the Investigation of Aerodynamic and Infrared Radiation Characteristics of a Flying Wing UAV. *Turbo Expo: Power for Land, Sea, and Air. American Society of Mechanical Engineers*, Vol. 84058, pp V001T01A042, 2020.
- [10]Cheng W, Wang Z, Zhou L, et al. Influences of shield ratio on the infrared signature of serpentine nozzle. *Aerospace Science and Technology*. Vol. 71, pp. 299-311, 2017.
- [11]Cheng W, Wang Z, Zhou L, et al. Investigation of Infrared Signature of Serpentine Nozzle for Turbofan. *Journal of Thermophysics and Heat Transfer*. Vol. 33, pp. 170-178, 2019.
- [12]P. Rajkumar, T. Chandra Sekar, A. Kushari, B. Mody, and B. Uthup. Flow Characterization for a Shallow Single Serpentine Nozzle with Aft Deck. *Journal of propulsion and power*, Vol. 33, No. 5, pp. 1130-1139, 2017.
- [13]H. Mohamed Abdelmotalib, C. Lee, Y. Seo, and J. Lee. A computational study of two-dimensional serpentine nozzle performance with different annular mixer configurations. *International Journal of Mechanical Sciences*, vol. 208, 2021.
- [14]Lee C, Boedicker C. Subsonic diffuser design and performance for advanced fighter aircraft. *Aircraft Design Systems and Operations Meeting*. 1985.
- [15]Anderson, J. D. *Modern Compressible Flow*. 3rd edition, McGraw-Hill, 2003.
- [16]Sun, Xiao-Lin, Wang, et al. Flow Characteristics of Double Serpentine Convergent Nozzle with Different Inlet Configuration. *Journal of engineering for gas turbines and power: Transactions of the ASME*, Vol. 140, 2018.